2014

State-space representation of the unsteady aerodynamics of flapping flight

Haithem E. Taha
Virginia Polytechnic Institute and State University, hezzat@vt.edu

Muhammad R. Hajj
Virginia Polytechnic Institute and State University, mhajj@vt.edu

Philip S. Beran
Wright-Patterson Air Force Base, philip.beran@wpafb.af.mil

Aerospace Science and Technology 34 (2014) 1–11

Contents lists available at ScienceDirect

Aerospace Science and Technology

www.elsevier.com/locate/aescte

State-space representation of the unsteady aerodynamics of flapping flight

Haithem E. Taha [a,*,1], Muhammad R. Hajj [a,2], Philip S. Beran [b,3]

[a] Virginia Polytechnic Institute and State University, Blacksburg, VA, 24061, United States
[b] U.S. Air Force Research Laboratory, Wright-Patterson Air Force Base, Ohio 45433, United States

ARTICLE INFO

Article history:
Received 14 October 2013
Received in revised form 23 January 2014
Accepted 28 January 2014
Available online 11 February 2014

Keywords:
Flapping flight
Leading Edge Vortex
Aspect ratio effects
Unsteady aerodynamics
Indicial response
Duhamel's principle

ABSTRACT

A state-space formulation for the aerodynamics of flapping flight is presented. The Duhamel's principle, applied in linear unsteady flows, is extended to non-conventional lift curves to capture the LEV contribution. The aspect ratio effects on the empirical formulae used to predict the static lift due to a stabilized Leading Edge Vortex (LEV) are provided. The unsteady lift due to arbitrary wing motion is generated using the static lift curve. Then, state-space representation for the unsteady lift is derived. The proposed model is validated through a comparison with direct numerical simulations of Navier–Stokes on hovering insects. A comparison with quasi-steady models that capture the LEV contribution is also performed to assess the role of unsteadiness. Similarly, a comparison with classical unsteady approaches is presented to assess the LEV dominance. Finally, a reduced-order model that is more suitable for flight dynamics and control analyses is derived from the full model.

1. Introduction

The aerodynamics of flapping flight have been the focus of research investigations for almost a century. The early studies were concerned with birds and insect flights and mainly carried out by biologists, such as Demoll [12,13]. More recently, there has been a significant interest in the modeling and simulation of flapping flights for design of micro-air-vehicles (MAVs). Flapping flight of MAVs/insects generates an unsteady nonlinear flow field that exploits non-conventional mechanisms to enhance the aerodynamic loads. Almost all of the early trials of explaining insect flight have invoked non-conventional high-lift mechanisms. Ellington et al. [20] explained how insects exploit the Leading Edge Vortex (LEV) as a high-lift mechanism, which is also known to be critical for lift generation of highly swept and delta wings aircraft. The LEV augments the bound vortex on the wing and, as such, the lift increases. This phenomenon is similar to the one observed in dynamic stall whereby the wing undergoes a rapid variation in the angle of attack. Yet, in contrast to dynamic stall, the LEV formed in insect flight has stable characteristics. This stability is attributed to an outward spanwise flow that convects the LEV towards the wing tip [20,54,53,61]. In the case of highly swept and delta wings, this spanwise flow is generated by the free-stream component parallel to the highly swept leading edge. In insect flight, similar to helicopters and propellers, the rotational motion creates a spanwise velocity gradient which, in turn, creates a pressure gradient that generates the spanwise flow.

Although the LEV is known to be the dominant contribution in insect flight, Dickinson et al. [15] indicated two other high-lift mechanisms, namely the rotational lift and wake-capture effects. The rotational lift is mainly due to the wing rotation at the end of each half stroke to adjust the angle of attack for the next half stroke. This rotational velocity of the wing creates a circulation that induces additional aerodynamic lift. On the other hand, Dickinson et al. observed peaks in the generated lift at the beginning of half strokes, when forward speed of the wing is almost zero. These peaks could not be explained by the previous two mechanisms. Dickinson et al. related these peaks to the lingering wake created during the previous half stroke. In addition to the non-conventional high-lift mechanisms discussed above, the role of unsteady aerodynamics in flapping flight is also quite significant. Other flow aspects that affect the aerodynamic loads include non-circulatory and viscous friction contributions. Unfortunately, it is very difficult to formulate a model for the aerodynamic forces that accurately captures all these phenomena without an expensive computational burden.

Over the two past decades, significant advancements have been made towards the understanding and modeling of the

* Corresponding author.
E-mail addresses: hezzat@vt.edu (H.E. Taha), mhajj@vt.edu (M.R. Hajj), philip.beran@wpafb.af.mil (P.S. Beran).
[1] Post-Doctoral Research Fellow, Engineering Science and Mechanics, Norris Hall.
[2] Professor, Engineering Science and Mechanics, Norris Hall.
[3] Principal Research Aerospace Engineer, AFRL/RBSD.

http://dx.doi.org/10.1016/j.ast.2014.01.011
1270-9638/

Nomenclature

AR	Aspect ratio
c	Chord length
$\bar{c}$	Mean chord length
C_D	Drag coefficient
C_L	Lift coefficient
$C_{L,s}$	Static lift coefficient
$\overline{C_L}$	Average lift coefficient
C_{L_α}	Lift curve slope of the three-dimensional wing
$C(k)$	Theodorsen function
$D(p)$	Theodorsen function in the Laplace-domain
k	Reduced frequency
ℓ	Lift per unit span
ℓ_s	Static lift per unit span
p	Laplace variable
r	Distance along the wing span
R	Wing radius (length)
Re	Reynolds number
S	Area of one wing
s, σ	Non-dimensional time variables
t, τ	Time variables
T, f	Flapping period and frequency
U	Air speed
$W(s)$	Wagner function
w	Wing normal velocity
ω	Flapping angular frequency
$\widehat{x}_0$	Normalized position of the pitch axis
α	Angle of attack
η	Pitching angle
φ	Back and forth flapping angle
ρ	Air density
ϑ	Plunging angle
LEV	Leading Edge Vortex
$UVLM$	The unsteady vortex lattice method

Table 1
The aerodynamic models in the literature that could be applied to hovering MAVs/insects and the physical aspects associated with the aerodynamics of flapping flight that each of the listed models captures along with the degrees-of-freedom associated with that model. UVLM refers to the unsteady vortex lattice method.

	Dickinson et al. [15]	Berman and Wang [8]	Peters et al. [39,34]	UVLM	Ansari et al. [5,6]	Proposed model
No. degrees-of-freedom	low	low	low	high	high	low
LEV contribution	✓	✓	×	×	✓	✓
Unsteadiness	×	×	✓	✓	✓	✓
Rotational lift	✓	✓	✓	✓	✓	✓
Added mass	✓	✓	✓	✓	✓	✓
Wake capture (hovering)	×	×	×	✓	✓	×
Viscous friction	×	✓	×	×	×	×

aerodynamics of flapping flight. For detailed reviews, the reader is referred to Mueller [31], Shyy et al. [46], Sane [42], Wang [57], and Ansari et al. [4]. Taha et al. [50] provided a review for the aerodynamic models specifically used in flight dynamics and control analyses. Table 1 lists the aerodynamic models that are available in the literature to be applied to hovering MAVs/insects. Also, we list the physical aspects associated with the aerodynamics of flapping flight that each of the listed models captures along with the degrees-of-freedom associated with that model. The first two models have algebraic forms and the third one comprises finite-state ordinary differential equations. The next two models involve simulation of the vortex kinematics at many locations on the airfoil surface and in its wake. Clearly, the first three models have a lower computational cost than the next two and hence are better-suited for flight dynamics and control analysis. Wang and Eldredge [59] proposed a remedy for the high computational cost associated with Ansari's model. Instead of shedding constant-strength point vortices at each time step from both leading and trailing edges, they shed variable-strength point vortices at larger time lapses. According to their shedding criterion, the strengths of the point vortices are determined at each time step by satisfying the Kutta condition at the edge it has shed from until an extremum value is reached. Then, the strength of this point vortex is kept constant and a new vortex is shed at this instant. This formulation greatly reduces the number of degrees-of-freedom. However, there is still a need to develop an unsteady model in a compact form that is suitable for aeroelasticity, flight dynamics, and control synthesis. Brunton and Rowley [10] considered Theodorsen's model of the lift frequency response [51] and modified its coefficients to be suitable for low Reynolds number regime. So, their final model has the same form as Theodorsen's but with different coefficients (different amplitudes). This cannot account for the LEV effect, which is our main concern in this work. Thus, it is concluded from Table 1 and the above discussion that there is a need for an aerodynamic model that captures the dominant LEV contribution along with the prominent unsteadiness with a feasible number of degrees-of-freedom so that it could be used in flight dynamics analysis, control synthesis, optimization, and sensitivity analysis.

More generally, Fig. 1 presents a taxonomy of the flapping flight regimes. For forward flights with a low reduced frequency k, typically $k < 0.1$, the quasi-steady aerodynamics is applicable. For forward flight with a relatively high k with local angles of attack up to 25°, a number of aerodynamic theories can be applied to capture the unsteadiness with a good accuracy either for two-dimensional or three-dimensional wings, e.g., Theodorsen [51], Shwarz and Sohngen (see [9]), Peters et al. [39,34,36,35,37,38], Jones [24–26], and Reissner [41]. In addition, methodologies such as the unsteady lifting line theory, the unsteady vortex lattice method, and the unsteady doublet lattice method can also be used to capture the unsteady effects on three-dimensional wings. On the other hand, for hovering with very high flapping frequency ω relative to the body natural frequency ω_n, it is generally assumed that there is no coupling between the periodic aerodynamic forces and the body natural modes [50]. As such, the body feels only the average forces, which might be predicted by the quasi-steady models that capture the dominant effect (LEV), for example, Dickinson et al. [15], Pesavento and Wang [33], and Andersen et al. [2,3]. For the middle regimes in Fig. 1, there is no aerodynamic model that could cover this gap with a feasible computational burden. The main characteristics of this regime are the LEV contribution, the prominent unsteadiness, and the coupling between the periodic aerodynamic forces and the body modes. The objective of this work is to develop a physics-based model in the form of ordinary-differential equations that describe the lift buildup during the flapping cycle, including the effect of the LEV on the aerodynamic loads. This model can provide better assessment of the flapping

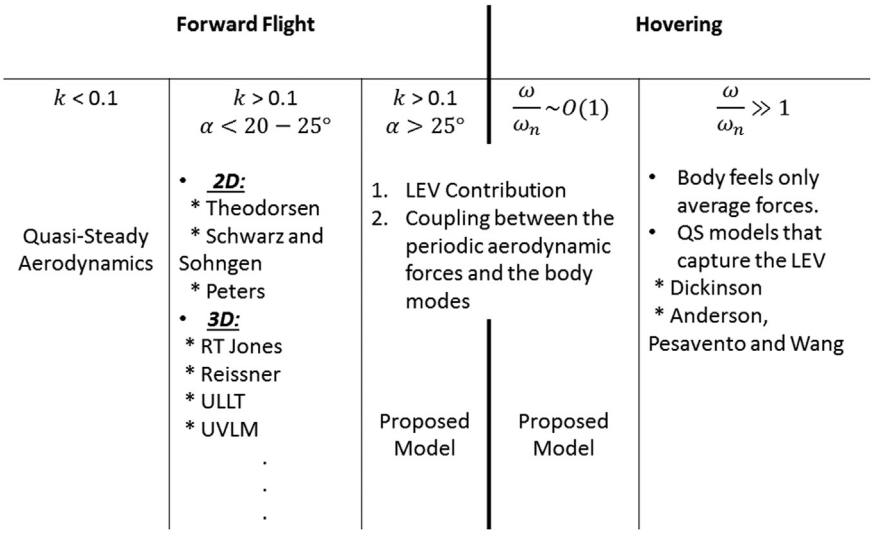

Fig. 1. Taxonomy of hovering and forward flight regimes. In forward flight, the reduced frequency $k = \frac{\omega c}{2U}$ is the key parameter to identify the region of application for each aerodynamic model. In hovering, the ratio of the flapping frequency ω to the body natural frequency ω_n is used to characterize the flight regimes.

flight dynamic stability, when augmented with the body equations of motion.

Motivated by developing such a model, we extend the Duhamel superposition principle, applied in unsteady linear aerodynamics, to flows with arbitrary C_L–α curves. This approach basically utilizes the static lift curve to determine the unsteady lift due to an arbitrary wing motion. A specific aspect of this work is the use of the quasi-steady circulation as the aerodynamic forcing input rather than the angle of attack or the airfoil speed. Hence, the developed model can be used to predict the temporal lift build up due to stabilized LEV, including the lag and phase shift associated with unsteady flows. We embed the effects of aspect ratio in the empirical formulae used to predict the static lift due to a stabilized LEV and, then, use them to construct the quasi-steady circulation (the aerodynamic forcing input to the developed unsteady model). Finally, a state-space representation of a complete unsteady aerodynamic model with application to hovering insects is provided. Validation of the derived model is performed through a comparison of time-histories of the modeled lift with corresponding results obtained by Sun and Du [49] solving Navier–Stokes equations for different insects. The results are also compared with those of the quasi-steady model of Berman and Wang [8] and those of the classical unsteady models.

2. Extension of Duhamel principle to arbitrary C_L–α curves

Because of their ability to capture the unsteady effects in a compact form, finite-state aerodynamic models have been used for aeroelastic and flight dynamic simulations and control design. The basis for most of the developed finite-state aerodynamic models is either Wagner's and/or Theodorsen's model for the unsteady lift. Wagner [56] obtained the time-response of the lift on a flat plate due to a step input (indicial response problem). Theodorsen [51] obtained the frequency response of the lift; that is, lift response due to a harmonically oscillating input, and applied it to the flutter problem of fixed-wing aircraft. Garrick [23] showed that the Wagner function, $W(s)$, and the Theodorsen function, $C(k)$, are related through the Fourier transform.

The principle underpinning this investigation is the Duhamel superposition principle. Wagner [56] determined the circulatory lift due to a step change in the wing motion. The unsteady lift is then written in terms of the static lift as

$$\ell(s) = \ell_s W(s) \tag{1}$$

where the non-dimensional time s is defined as $s = \frac{2Ut}{c}$ for constant free-stream velocity U and defined as

$$s = \frac{2}{c}\int_0^t U(\tau)\,d\tau \tag{2}$$

for varying free-stream $U(\tau)$ in this work. As for the dynamic lift, knowing the indicial response for a linear dynamical system, the response due to arbitrary excitation (input) can be written as an integral (superposition) using the indicial response and time-variation of the input variable. As such, the variation of the circulatory lift due to an arbitrary change in the angle of attack is expressed as

$$\ell(s) = \pi\rho U^2 c\left(\alpha(0)W(s) + \int_0^s \frac{d\alpha(\sigma)}{d\sigma} W(s-\sigma)\,d\sigma\right) \tag{3}$$

We note that $W(s)$ can also be used as an indicial response to aerodynamic inputs other than the angle of attack. Van der Wall and Leishman [55] used it as an indicial response to the wing normal velocity, $w = U\alpha$, in the case of time-varying free stream. For a relatively high angle of attack, the Duhamel superposition is performed using a more exact normal velocity $w = U\sin\alpha$. Eq. (3) is then re-written as

$$\ell(s) = \pi\rho U(s) c\left(U(0)\sin\alpha(0)W(s) + \int_0^s \frac{d(U(\sigma)\sin\alpha(\sigma))}{d\sigma} W(s-\sigma)\,d\sigma\right) \tag{4}$$

This equation is usually used in dynamic stall models where relatively high α's are encountered, e.g., the Beddoes–Leishman dynamic stall model developed in [7,28,30,29].

The main issue with the classical unsteady formulations discussed above is their inability to account for a non-conventional lift curve (lift mechanism), such as the LEV contribution. To remedy this, we note that the above discussion presumes linear dependence of the lift on α, $U\alpha$, or $U\sin\alpha$. Within the framework of potential flow, the lift is linearly dependent on the circulation. This linear dependence presents the possibility of generalizing

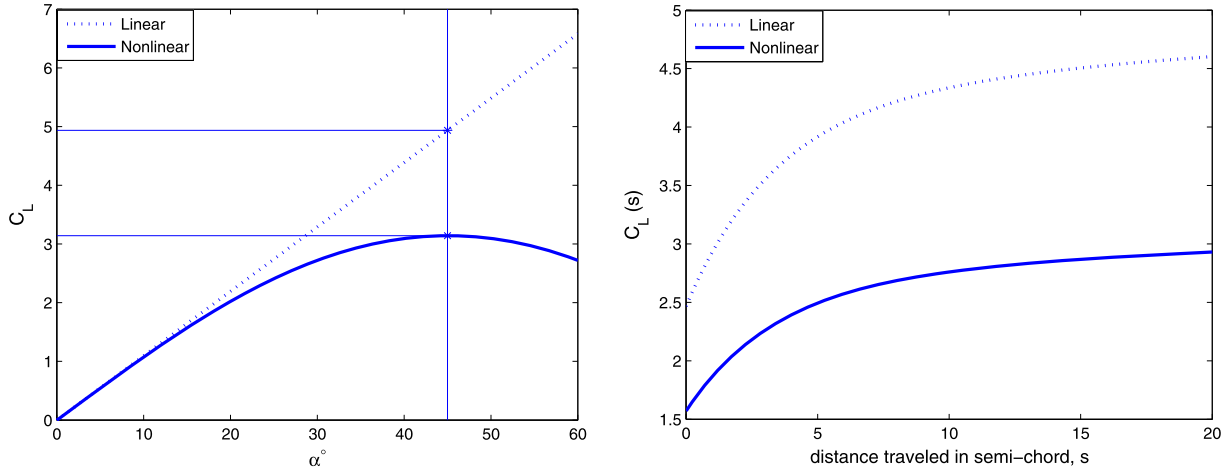

(a) Static lift variation with the angle of attack (b) Lift build up

Fig. 2. Linear and nonlinear lift build up.

Eq. (4) for an arbitrary lift curve using the circulation as an aerodynamic forcing input in the Duhamel integral. As such, we write the Duhamel's integral as

$$\ell(s) = \rho U(s)\left(\Gamma_{QS}(0)W(s) + \int_0^s \frac{d\Gamma_{QS}(\sigma)}{d\sigma} W(s-\sigma)\,d\sigma\right) \tag{5}$$

where Γ_{QS} is the quasi-steady circulation. For a translating wing, $\Gamma_{QS}(s) = \frac{1}{2}cU(s)C_L(s)$, where the static lift curve is used to predict $C_L(s)$; i.e., $C_L(s) \equiv C_{L,s}(\alpha(s))$. Eq. (5) is the extension of the unsteady aerodynamic modeling using Duhamel superposition to arbitrary static C_L–α curves, and arbitrary-varying free-stream $U(s)$. It should be noted that Eq. (5) reduces to all the previous forms of Duhamel superposition for the particular cases of interest. Moreover, Eq. (5) allows us to account for the instantaneous rotational effects ($\dot{\alpha}$-effects). This can be achieved by splitting the translational component from the rotational one and writing the total circulation as the sum of the two terms, i.e., $\Gamma = \Gamma_{trans} + \Gamma_{rot}$. As for Γ_{rot}, one could use the potential flow result of a pitching airfoil, see [22]

$$\Gamma_{rot} = \pi c^2 \dot{\alpha}\left(\frac{3}{4} - \widehat{x}_0\right) \tag{6}$$

This splitting is justified as Eq. (6) matches well the experiments of Dickinson et al. [15], Sane and Dickinson [43] and Andersen et al. [2].

The main assumption here is that the lift response to an increment in circulation is independent of the aerodynamic state and the Wagner function could be used to represent the indicial response of the circulatory lift even for high values of α; that is, Eq. (1) is still valid for high values of α. In other words, it is assumed that the nonlinearity of the C_L–α curve is accounted for in the steady circulation term (input) and does not affect the temporal build up of the circulatory lift, as illustrated in Fig. 2 for a constant free stream. Fig. 2(a) shows static linear and nonlinear lift curves, from which the C_L values at a certain angle of attack, α, are picked. Fig. 2(b) shows the corresponding lift build up to these values. It is assumed that both the linear and nonlinear lift exhibit the same temporal lift build up but to different values; ones corresponding to the static lift curves.

To be more suitable for dynamic stability analysis and control synthesis, Eq. (5) would be written in a state-space form. For constant U, we could use a finite-state approximation for $W(s)$, e.g., R.T. Jones [24] or W.P. Jones [27], which presents $W(s)$ on the form

$$W(s) = 1 - A_1 e^{-b_1 s} - A_2 e^{-b_2 s} \tag{7}$$

Then, we can use Laplace transform to get a transfer function and consequently to obtain the corresponding state-space model. However, for a variable free-stream, the targeted state-space model is expected to have time-varying coefficients, which eliminates the ability to use the Laplace transform. Rewriting Eq. (5) in terms of the dimensional time variables, t and τ, and integrating the second term by parts, we obtain

$$\begin{aligned}\ell(t) &= \rho U(t)\Gamma_{eff}(t)\\ &= \rho U(t)\left(\Gamma_{QS}(t)W(0) - \int_0^t \Gamma_{QS}(\tau)\frac{dW(t-\tau)}{d\tau}\,d\tau\right)\end{aligned} \tag{8}$$

where Γ_{eff} is the effective unsteady circulation. Using the two-state approximation of the Wagner function as presented in Eq. (7) and recalling the definition of the non-dimensional time from Eq. (2), the term $\frac{dW(t-\tau)}{d\tau}$ is written as

$$\frac{dW(t-\tau)}{d\tau} = -A_i \frac{2b_i}{c} U(\tau) e^{\frac{-2b_i}{c}\int_\tau^t U(\tau)\,d\tau}, \quad i = 1,2 \tag{9}$$

where summation on the repeated indexes is used. Thus, Γ_{eff} is given by

$$\Gamma_{eff}(t) = (1 - A_1 - A_2)\Gamma_{QS}(t) + x_i(t), \quad i = 1,2 \tag{10}$$

where x_i is written as

$$x_i(t) = \int_0^t U(\tau) A_i \frac{2b_i}{c} U(\tau) e^{\frac{-2b_i}{c}\int_\tau^t U(\tau)\,d\tau}\,d\tau, \quad i = 1,2 \tag{11}$$

Eq. (11) represents solution to the linear differential equation

$$\dot{x}_i(t) = \frac{2b_i U(t)}{c}\big(-x_i(t) + A_i \Gamma_{QS}(t)\big), \quad i = 1,2 \tag{12}$$

with $x_i(0) = 0$. In conclusion, the circulatory lift per unit span is written as

$$\ell(t) = \rho U(t)\big[(1 - A_1 - A_2)\Gamma_{QS}(t) + x_1(t) + x_2(t)\big] \tag{13}$$

where the state equations for x_1 and x_2 are given in Eq. (12) and $\Gamma_{QS}(t)$ is given by

$$\Gamma_{QS}(t) = \frac{1}{2}cU(t)C_{L,s}\big(\alpha(t)\big) + \pi c^2\left(\frac{3}{4} - \widehat{x}_0\right)\dot{\alpha}(t) \tag{14}$$

Any arbitrary wing motion $(U(t), \alpha(t))$ along with any arbitrary nonlinear $C_{L,s}$–α curve can be plugged into Eq. (14) to obtain the time variation of the quasi-steady circulation $\Gamma_{QS}(t)$. This term is, in turn, considered as a forcing term in the state-space model, Eq. (12). The circulatory lift per unit span, ℓ, is then determined from Eq. (13).

3. Application to hovering insects

Since the developed unsteady model requires a priori knowledge of the static lift curve, the next subsection provides a generalization for the empirical formulae to predict the static lift due to a stabilized LEV accounting for the aspect ratio effects.

3.1. Static lift due to a stabilized LEV-effect of aspect ratio

Due to its compactness, the model of Dickinson et al. [15] has been extensively used in dynamics and control of flapping MAVs, e.g., [47,48,44,14,16,32]. It is a quasi-static expression; i.e., it gives an algebraic expression for the lift and drag coefficients as functions of the instantaneous angle of attack

$$C_L = 0.225 + 1.58\sin(2.13\alpha - 7.20)$$
$$C_D = 1.92 - 1.55\cos(2.04\alpha - 9.82) \tag{15}$$

Wang et al. [58] fit their data with simpler forms; $C_L = A\sin 2\alpha$, $C_D = B - C\cos 2\alpha$ or $C_D = C_D(0)\cos^2\alpha + C_D(\frac{\pi}{2})\sin^2\alpha$, where the coefficients $A, B, C, C_D(0)$, and $C_D(\frac{\pi}{2})$ were determined experimentally.

There are two fundamental shortcomings with the quasi-steady models mentioned above. Firstly, they do not account for the unsteady aspects associated with flapping flight. Secondly, the coefficients describing the aerodynamic terms in these models are determined empirically and typically do not account for any variations in the wing shape. This latter concern can best be explained by considering the work of Polhamus [40] who was the first to model the LEV contribution on highly swept and delta wings by a leading edge suction analogy. He identified two components for the lift, namely the potential flow lift with zero leading edge suction, $C_{Lp} = K_p \sin\alpha\cos^2\alpha$, and the vortex lift $C_{Lv} = K_v \cos\alpha\sin^2\alpha$. Both K_p and K_v are functions of the aspect ratio (AR). Particularly, K_p, which becomes the lift curve slope in the limit of small angles of attack, is a strong function of the AR. Since Polhamus' formula models the same phenomenon (a stabilized LEV) as the previously mentioned quasi-steady models such as Dickinson's model, Eq. (15), the coefficients in these models would not be valid for any arbitrary wing, as those coefficients could considerably change with variations in the AR. In this section, we a general formula for these coefficients in terms of the wing AR.

Wang et al. [58] showed that the static lift coefficient for a translating wing, taking into account the LEV effect, could be fit by $C_L = A\sin 2\alpha$ where A is a constant coefficient. Berman and Wang [8] provided values for A for the hawk moth, bumblebee, and fruit fly. However, there are no general formulas for this coefficient as a function of the wing geometry. In the limit to small angles, the formula by Wang et al. reduces to $C_L = 2A\alpha$; i.e., $2A$ may be considered as the lift curve slope of the three-dimensional wing C_{L_α}. Since flapping flight is associated with low aspect ratio wings, one can use the *Extended Lifting Line Theory* (Schlichting and Truckenbrodt [45]) to obtain the dependence of C_{L_α} on the wing AR, which is given by

$$C_{L_\alpha} = \frac{\pi AR}{1 + \sqrt{(\frac{\pi AR}{a_0})^2 + 1}} \tag{16}$$

Table 2
Morphological and aerodynamic parameters for the four insects studied.

Insect	R (mm)	S (mm^2)	Aspect ratio	A
Drosophila virilis	3	2.97	3.10	–
Hawk moth	51.9	947.8	2.84	1.678
Bumble bee	13.2	54.9	3.17	1.341
Fruit fly	2.02	1.36	3.00	1.833

with the AR being based on one wing; i.e., $AR = \frac{R^2}{S}$, and a_0 is the lift curve slope of the two-dimensional airfoil section, e.g. it is equal to 2π for a flat plate or a very thin cambered shape. For conventional airfoils, it could be determined from lift curves such as the ones presented by Abbott and Doenhoff [1]. Using Eq. (16), the static lift coefficient can be written as

$$C_L = \frac{\pi AR}{2(1 + \sqrt{(\frac{\pi AR}{a_0})^2 + 1})}\sin 2\alpha \tag{17}$$

A comparison is performed among the C_L–α curve using Eq. (17), Polhamus' formula, the potential flow lift coefficient $C_L = C_{L_\alpha}\sin\alpha$, and benchmark results for four insects: Drosophila virilis, Hawk moth, Bumble bee, and Fruit fly. Eq. (16) was used to determine C_{L_α} in Polhamus' formula ($K_p \equiv C_{L_\alpha}$) and the potential flow equation. As for the coefficient K_v in Polhamus' formula for the lift due to LEV, the expression given in [40]

$$K_v = \left(K_p - K_p^2 K_i\right)\frac{1}{\cos\Lambda} \tag{18}$$

is adopted, where $K_i = \frac{\partial C_{D,induced}}{\partial C_L^2}$, which can be taken as $\frac{1}{\pi AR}$ for elliptic wings, and Λ is the sweep angle, which is assumed to be zero. Dickinson's empirical model, Eq. (15), was used to obtain the benchmark C_L in Fig. 3(a) for the Drosophila virilis wing which was used as the basis for their empirical model in [15]. For the other three insects, the formula of Wang et al. $C_L = A\sin 2\alpha$ was used to obtain the benchmark C_L, taking the values of A provided by Berman and Wang [8] for those insects. Table 2 lists the morphological parameters (R, S and AR) for the four insects, and the aerodynamic parameter A for the three insects given in [8].

The divergence observed in Fig. 3 between the potential flow lift and the benchmark results for all insects at relatively high values of α is expected. Although Polhamus [40] did not verify his results for this wide range of α, his approach shows a good agreement with the benchmark results. However, the proposed formula, Eq. (17), is quite simpler and yields C_L values that are closer to the benchmark results than those of Polhamus for all insects.

The bumble bee case deserves a more thorough discussion. We showed two benchmark results in Fig. 3(c), namely, those of Berman and Wang [8] and Usherwood and Ellington [52]. Berman and Wang obtained the coefficient A by fitting the data of Dudley and Ellington [17], which were for steady forward flight not hovering. That is, these data were for a completely fixed wing in a wind tunnel, not a revolving wing like that of the experiments of Dickinson et al. [15] or Usherwood and Ellington [52]. This may be the reason for the relatively larger discrepancy between the estimated C_L by Berman, and Wang, and the one predicted by Eq. (17) and that of Polhamus' formula. It should be noted that Usherwood and Ellington [52] provided two sets of C_L-measurements. They categorized them into *early* and *steady* measurements. The early set represents measurements during the first half revolution of the wing from the start time excluding transients. The steady set represents measurements from 180° to 450° (from half to one and a half revolutions). Since a steady rotation (not back and forth flapping) is considered in the experiment, the early measurements are taken before the propeller wake and downwash are fully developed

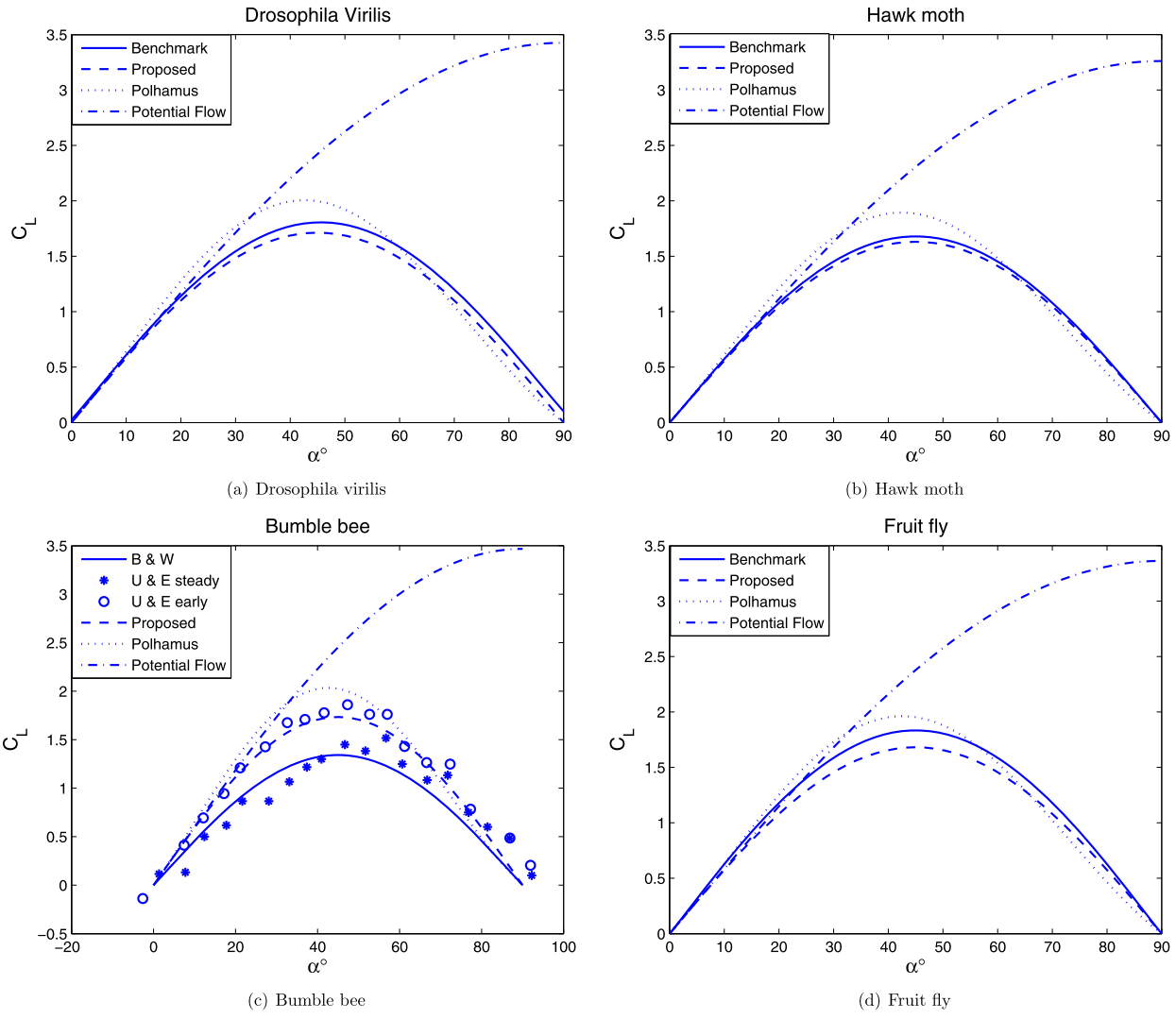

(a) Drosophila virilis (b) Hawk moth

(c) Bumble bee (d) Fruit fly

Fig. 3. Comparison between the proposed formula, Polhamus, potential flow, and benchmark results for C_L due to a stabilized LEV.

and steady conditions are reached. Hence, Usherwood and Ellington suggested the use of the early set for analysis of flapping flight. The C_L values predicted by Eq. (17) are in a better agreement with the early results of Usherwood and Ellington than those of Berman and Wang. On the contrary, the estimated C_L by Berman and Wang is closer to the steady results of Usherwood and Ellington. In conclusion, Eq. (17) has been shown to provide a surrogate model that accounts for the *AR* effects on the lift due to a stabilized LEV.

3.2. Unsteady lift

In flapping-wing flight, the flapping kinematics with respect to the body is usually described by the three Euler angles: the back and forth flapping angle φ, the plunging angle ϑ, and the pitching angle η. However, it can be assumed that most insects hover in a horizontal stroke plane without an out-of-plane motion ($\vartheta = 0$) as stated by Weis-Fogh [60] and Ellington [19]. Fig. 4 shows a schematic diagram for a flapping MAV whose wings sweep a horizontal plane. The axis-system x_b, y_b, and z_b is a body-fixed frame and the system x_w, y_w, and z_w is a wing-fixed frame. Two rotations are considered, in this work, from the body-frame to the wing-frame; that is φ and η. The flapping angle φ is the rotation about the z_b-axis and the pitching angle η is the rotation about the y_w-axis. As such, the total flapping velocity, seen by an airfoil section that is a distance r from the wing root, is $r\dot{\varphi}$ with the angle of attack given by

$$\alpha(t) = \begin{cases} \eta, & \dot{\varphi} > 0 \\ \pi - \eta, & \dot{\varphi} < 0 \end{cases} \tag{19}$$

Hence, according to the unsteady finite-state model developed above, the instantaneous lift per unit span on that airfoil section is given by

$$\ell(r,t) = \ell_{NC}(r,t) + \rho r\left|\dot{\varphi}(t)\right| \times \left[(1 - A_1 - A_2)\Gamma_{QS}(r,t) + x_1(r,t) + x_2(r,t)\right] \tag{20}$$

where the non-circulatory lift component, ℓ_{NC}, is given by

$$\ell_{NC}(r,t) = -m_{app}(r)a_y(r,t)\cos\eta(t) \tag{21}$$

where $m_{app}(r) = \frac{\pi}{4}\rho c^2(r)$ is the apparent mass of the two-dimensional strip, $a_y(r,t)$ and $\Gamma_{QS}(r,t)$ are the airfoil upward normal acceleration and the quasi-steady circulation, respectively, and are given by

$$a_y(r,t) = r\left(-\ddot{\varphi}(t)\sin\eta(t) - \dot{\varphi}(t)\dot{\eta}(t)\cos\eta(t)\right)$$
$$\Gamma_{QS}(r,t) = \frac{1}{2}c(r)r\dot{\varphi}(t)C_{L,s}\left(\eta(t)\right) + \pi c^2(r)\left(\frac{3}{4} - \widehat{x}_0\right)\dot{\eta}(t) \tag{22}$$

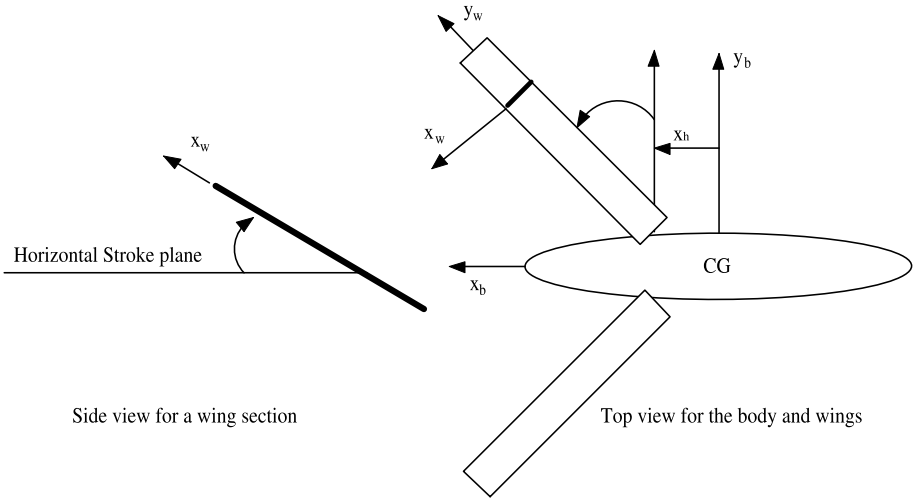

Fig. 4. Schematic diagram for a flapping-wing MAV whose wings sweep a horizontal plane.

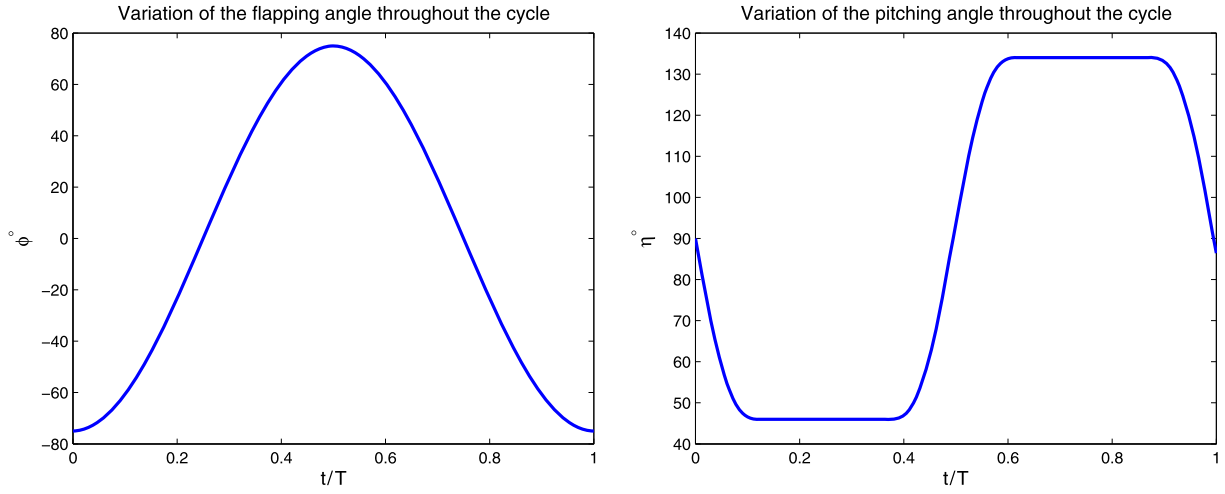

(a) Variation of the back and forth flapping angle φ

(b) Variation of the pitching angle η

Fig. 5. The hovering idealized kinematics used by Sun and Du [49] for the fruit fly case.

where, for hovering MAVs having LEV shed, it has been shown in the previous subsection that Eq. (17) is sufficient to predict the static lift coefficient $C_{L,s}$ of the three-dimensional wing. Finally, the dynamics of the internal flow-states x_1 and x_2 are governed by

$$\dot{x}_i(r,t) = \frac{2b_i r|\dot{\varphi}(t)|}{c(r)}\left[-x_i(r,t) + A_i \Gamma_{QS}(r,t)\right], \quad j = i = 1,2 \quad (23)$$

The three-dimensionality is accounted for by using strip theory and $C_{L,s}$ of the three-dimensional wing. If dynamic twist is allowed, however, $C_{L,s}$ will have to be of the two-dimensional strip and a three-dimensional correction for the lift curve slope may be used instead.

4. Validation and comparison with previous models

Validation of the aerodynamic loads as predicted by the proposed model is performed by comparing its results to those obtained by Sun and Du [49]. They performed direct numerical simulation (DNS) for Navier–Stokes equations on the wings of different insects that cover a wide range of operating conditions and morphological parameters. According to the above model, the lift force is driven by the wing kinematic functions, φ and η. Sun and Du considered idealized kinematics without an out-of-plane motion ($\vartheta = 0$) that closely match the observed kinematics in nature, as described by Dickinson et al. [15]. Their kinematics prescribe the flapping angle to be a simple harmonic: $\varphi(t) = -\frac{\Phi}{2}\cos(\omega t)$, where $\frac{\Phi}{2}$ is the flapping amplitude. As for the pitching angle, η, it takes a constant value, referred to as α_m, except at the beginning and near the end of each half stroke. During the rotation phase, the η variation is described by

$$\eta(t) = \frac{\Delta\alpha}{\Delta t_r}\left[(t - t_r) - \frac{\Delta t_r}{2\pi}\sin\left(\frac{2\pi(t - t_r)}{\Delta t_r}\right)\right] \quad (24)$$

where Δt_r is the duration of each rotational phase, and t_r is the time at which this phase starts. Knowing α_m is enough to determine $\Delta\alpha$, since the wing rotates from α_m to $\pi - \alpha_m$ or vice versa. Setting Δt_r equal to $0.25T$, and considering symmetric rotation, t_r can be determined. Fig. 5 shows the variation of the kinematic angles φ and η throughout the flapping cycle for the fruit fly case. As for the wing planform, one just needs the chord distribution, or more specifically the weighted moments of the wing area. The values of these moments can be found in [21] for the fruit fly and in [18] for all other insects. Sun and Du listed all the required morphological parameters, f, Φ, α_m, S, R, and the total mass for all the insects under study.

To further emphasize the physical aspects captured by the developed model, we compare its results to the most recent quasi-steady model of Berman and Wang [8] which is based on Andersen

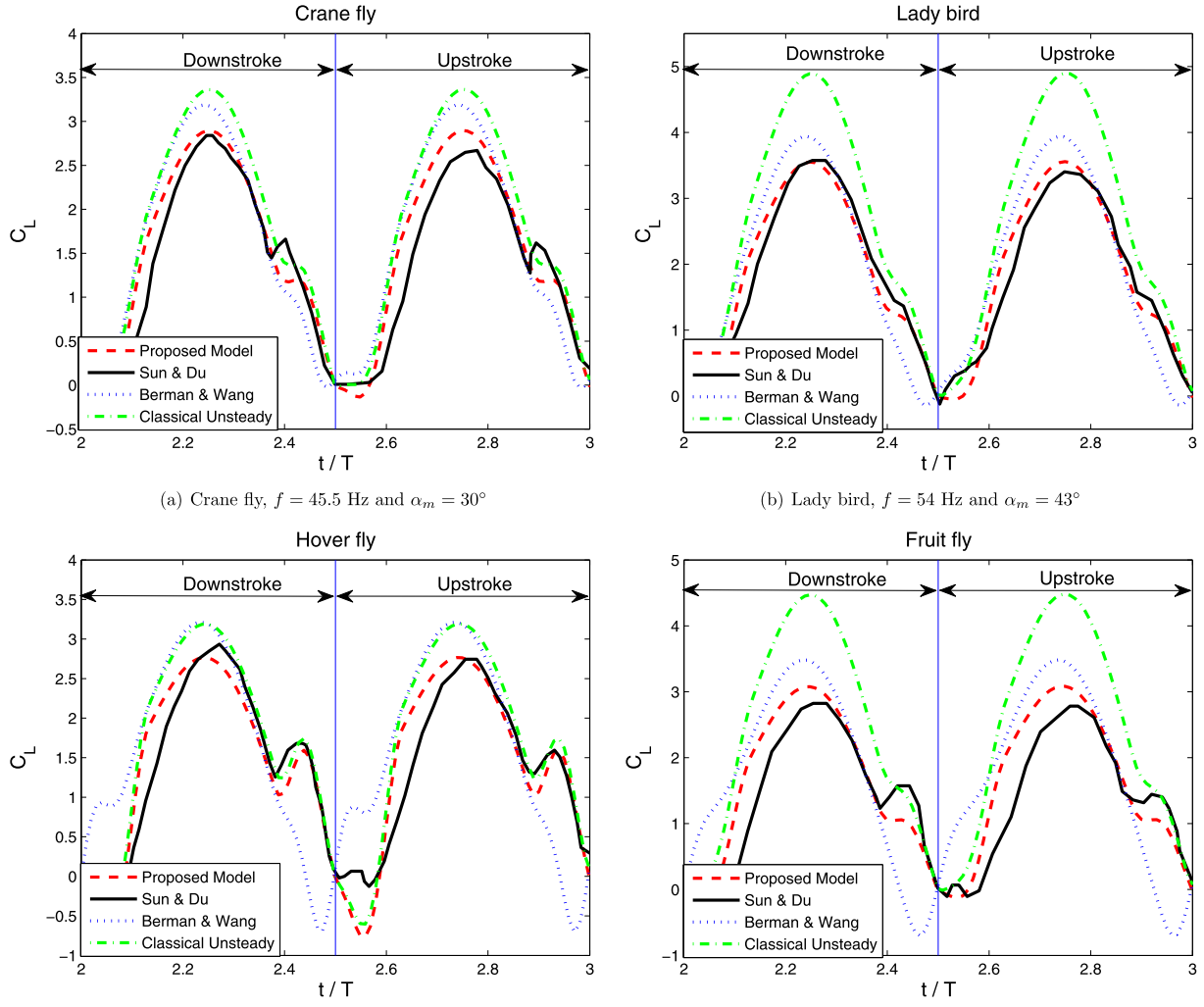

(a) Crane fly, $f = 45.5$ Hz and $\alpha_m = 30°$

(b) Lady bird, $f = 54$ Hz and $\alpha_m = 43°$

(c) Hover fly, $f = 160$ Hz and $\alpha_m = 29°$

(d) Fruit fly, $f = 254$ Hz and $\alpha_m = 46°$

Fig. 6. Comparison of the C_L over one flapping cycle using the current state-space model, the DNS results of Sun and Du [49], the quasi-steady model of Berman and Wang [8], and the classical unsteady approach for four insects.

et al. [2,3] and Pesavento and Wang [33]. This comparison is expected to show the effects of unsteadiness on the aerodynamics of flapping flight. Moreover, we present a comparison with the classical unsteady approach; i.e., the state-space formulation of Eq. (4) along with the added mass contribution. This model is described in details in [30,29]. This comparison is expected to assess the effects of the LEV on the aerodynamics of flapping flight. It should be noted that, because of the low aspect ratio of insect wings, keeping the lift curve slope at 2π like the classical unsteady approach shown in Eq. (4), leads to highly erroneous results (almost doubles the aerodynamic loads). So, we opted to use the three-dimensional lift curve slope as presented in Eq. (16) in the classical unsteady formulation as well to make the comparison more meaningful.

Fig. 6 shows a comparison of the steady-state periodic variation of the lift coefficient over one cycle for the four insects studied by Sun and Du. The lift coefficient is based on the reference speed adopted by Sun and Du, $U_{ref} = 2f\Phi r_2$, where r_2/R is the non-dimensional second moment of wing area. As such, the lift coefficient is defined as $C_L = \frac{L}{\rho U_{ref}^2 S}$. It should be emphasized that despite the complexity of the flow field and the simplicity and compactness of the proposed model, it is able to capture the LEV contribution in an unsteady fashion as the lift variation throughout the cycle matches well the benchmark results for all the insects.

It is very well known that quasi-steady models predict higher loads than their unsteady counterparts, see [11] for example. This illustrates the reason behind the higher C_L-values predicted by the model of Berman and Wang. Its unsteady counterpart (the present model) is closer to the DNS results of Sun and Du. The largest deviation amongst the four insects of the quasi-steady model of Berman and Wang from the present and the DNS results takes place in the case of fruit fly ($f = 254$ Hz). This is consistent with the fact that the deviation of quasi-steady models from their unsteady counterparts is more pronounced at higher frequencies. On the other hand, the steady values for C_L due to a stabilized LEV are less than those predicted by the classical potential flow formula $C_L = C_{L_\alpha} \sin\alpha$, as shown in Fig. 3, particularly for angles of attack higher than 25°. This illustrates the reason behind the higher C_L-values predicted by the classical unsteady approach in the middle of half strokes where the LEV contribution is dominant. Deviations of the classical unsteady results from the present and the DNS ones are larger in the cases of $\alpha_m = 46°$ and 43 (fruit fly and ladybird) in comparison to the cases of $\alpha_m = 29°$ and 30 (hover fly and crane fly). This is consistent with the fact that the deviation of the classical potential flow theory from the true LEV steady C_L–α curve becomes larger as the angle of attack is increased, see Fig. 3. It should be noted that, however, near stroke reversals where the effect of wing rotation becomes dominant, the

Table 3
The operating conditions for the four insects under study along with the two comparison metrics $\Delta\overline{C_L}$ and $\Delta C_{L_{rms}}$ between each of the three studied models and the DNS results. The numbers given between parenthesis are for $\Delta C_{L_{rms}}$.

Insect	Φ°	α_m°	f (Hz)	Present model	Classical unsteady	Berman and Wang
Crane fly	123	30	45.5	7.3 (7.9)	26.9 (15.5)	13.12 (14.6)
Lady bird	177	43	54	1.8 (5.8)	43.1 (22.0)	7.0 (12.7)
Hover fly	90	29	160	3.4 (10.4)	14.0 (13.6)	8.6 (25.2)
Fruit fly	150	46	254	0.3 (12.8)	49.2 (36.2)	16.9 (31.6)

classical unsteady approach predicts C_L-values that are very close to the present results and the DNS results. Note that they have the same models for rotational contributions.

It is noted from Fig. 6 that the quasi-steady model of Berman and Wang is closer to the present results and the DNS results than the classical unsteady approach in the middle of half strokes where the LEV contribution is dominant. However, its performance is poorer near stroke reversals where the rotational contribution is dominant. Thus, for symmetric flapping (identical downstroke and upstroke) where the net rotational contribution to the cycle-average lift is zero, the quasi-steady models of Berman and Wang or Dickinson et al. [15] might result in good estimates for the cycle-average lift coefficients. This notion along with their compactness make them suitable for performing preliminary designs of flapping-wing MAVs. However, because they perform poorly near stroke reversals, these models are not satisfactory when used to perform aerodynamic optimization that may depend on rotational contributions or to analyze asymmetric flapping cycles necessary for control purposes. It is noteworthy to mention that because the present model is intended to be a blend of the quasi-steady models (capturing the LEV contribution) and the classical unsteady representations, its results are always closer to the better model in its region of applicability; i.e., closer to the quasi-steady model in the middle of half strokes and closer to the unsteady model near stroke reversals.

Table 3 presents the operating conditions for the four insects under study along with two comparison metrics between each of the three studied models and the DNS results. These metrics are the percentage deviation in cycle average lift coefficient from the DNS value $\Delta\overline{C_L}\% = \frac{|\overline{C_L}_{model} - \overline{C_L}_{DNS}|}{\overline{C_L}_{DNS}} \times 100$ and the root-mean-squared difference of the lift coefficient in percent of maximum lift coefficient $\Delta C_{L_{rms}}\% = \frac{\sqrt{\frac{1}{T}\int_0^T (C_{L_{model}}(t) - C_{L_{DNS}}(t))^2\,dt}}{\max(C_{L_{DNS}})} \times 100$. Both metrics show that the performance of the present model is better than the other two models. It should be also emphasized that the computational cost of the three models under study are almost the same. Therefore, using the present model allows capturing non-conventional lift curves/mechanisms (LEV) in an unsteady fashion without an extra computational burden. Finally, it is noteworthy to mention that using the two-dimensional lift-curve slope 2π as in Eq. (4) leads to very large deviations of the classical unsteady approach. In terms of the stated comparison metrics, it leads to $\Delta\overline{C_L}\% = 85.5, 150.9, 86.0, 183.6$ and $\Delta C_{L_{rms}}\% = 43.4, 75.9, 46.6, 111.0$ for the four insects, respectively.

Finally, it should be noted that the developed model will not be applicable in the cases where unstable leading edge vortices are encountered. This may happen at relatively high Reynolds numbers and/or in cases of wings with thick, rounded leading edges. Noting that the flapping wings are naturally very thin having sharp leading edges, we also point to the fact that the largest Reynolds number of flying insects of interest (Hawk moth) is 3852 for which the LEV is still of a stable nature. In addition, in contrast to fixed wings, the spanwise flow on flapping wings induces a stabilizing action to the formed LEV. Thus, the flapping flight will mostly be associated with a stabilized LEV.

5. Reduced-order modeling

The above calculations were performed using 50 spanwise stations, which required a total of 100 aerodynamic states. However, flight dynamicists may wish to have a more reduced-order model in terms of the internal aerodynamic states that is more suitable for flight dynamics and control analyses without loss of the physics being captured.

Motivated by such a goal, we propose a fourth order model that still captures the same physical aspects (LEV, unsteadiness, and rotational contributions). This is achieved by exploiting the knowledge of the spanwise distributions of all the lift contributors in the integration of Eq. (20) over the wing. This dictates the separation of the translational term from the rotational one because the two terms have different spanwise distributions: $r^2c(r)$ for the translational term versus $rc^2(r)$ for the rotational term. As such, the total lift on the wing is written as $L = L_{NC} + L_{trans} + L_{rot}$ where

$$L_{NC}(t) = \frac{\pi}{4}\rho I_{12}\big[\ddot{\varphi}(t)\sin\eta(t) + \dot{\varphi}(t)\dot{\eta}(t)\cos\eta(t)\big]\cos\eta(t)$$

$$L_{trans}(t) = \frac{1}{2}\rho I_{21}\big|\dot{\varphi}(t)\big| \times \big[(1 - A_1 - A_2)\dot{\varphi}(t)C_{L,s}\big(\eta(t)\big) + x_1(t) + x_2(t)\big]$$

and

$$L_{rot}(t) = \rho I_{12}\left(\frac{3}{4} - \widehat{x}_0\right)\dot{\varphi}(t)\big[(1 - A_1 - A_2)\dot{\eta}(t) + x_3(t) + x_4(t)\big] \tag{25}$$

where $I_{21} = 2\int_0^R r^2c(r)\,dr$, and $I_{12} = 2\int_0^R rc^2(r)\,dr$ are the weighted moments of area for the two wing halves. The state equations for the four state variables are then given by

$$\dot{x}_i(t) = \frac{2b_j\bar{r}|\dot{\varphi}(t)|}{\bar{c}}\big[-x_i(t) + A_j\dot{\varphi}(t)C_{L,s}\big(\eta(t)\big)\big], \quad j = i = 1, 2$$

$$\dot{x}_i(t) = \frac{2b_j\bar{r}|\dot{\varphi}(t)|}{\bar{c}}\big[-x_i(t) + A_j\dot{\eta}(t)\big], \quad j = i - 2 = 1, 2 \tag{26}$$

where $\bar{r}$ and $\bar{c}$ are taken at a certain reference section. For the plots shown below, we use the section at $r = r_2 = \frac{I_{21}}{2SR}$ as a reference section.

Fig. 7 shows a comparison between the lift coefficient obtained by using the reduced-order model (four states) and that using the full model (100 states). The plots show a very good agreement. Additionally, in terms of the comparison metrics, the following deviations for the reduce-order model from the DNS results are found 12.0 (6.3), 2.0 (5.6), 10.3 (10.6), and 4.3 (12.3). Hence, the reduced-order model could capture the dominant contributions of the aerodynamic loads with a quite feasible computational burden. Moreover, it is represented in a compact form that is very well suited for flight dynamic stability and control analyses of flapping-wing MAVs. Finally, we should note that a similar agreement is obtained when using the section having the mean chord length as a reference section.

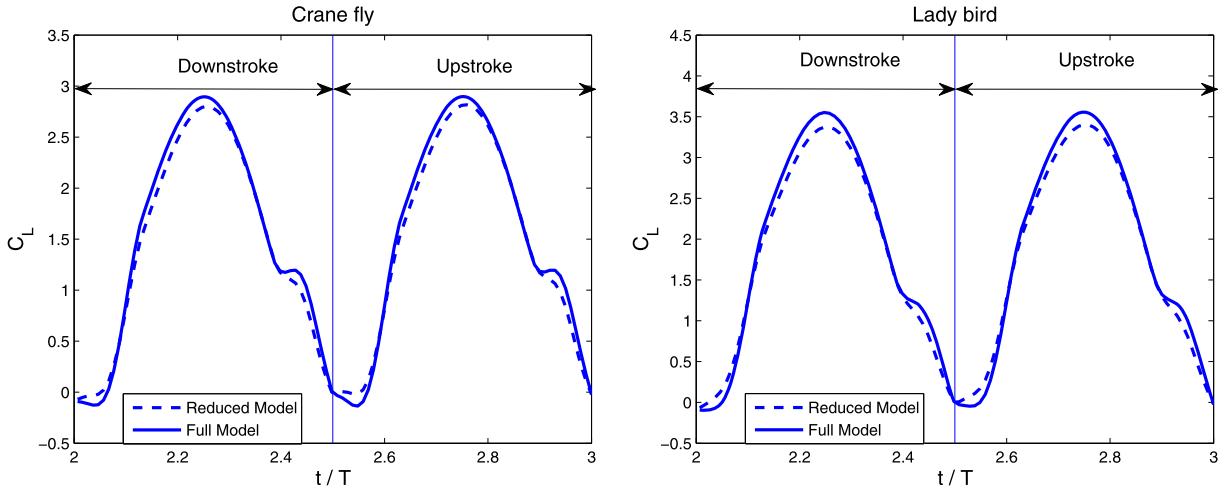

(a) Crane fly, $f = 45.5$ Hz and $\alpha_m = 30°$

(b) Lady bird, $f = 54$ Hz and $\alpha_m = 43°$

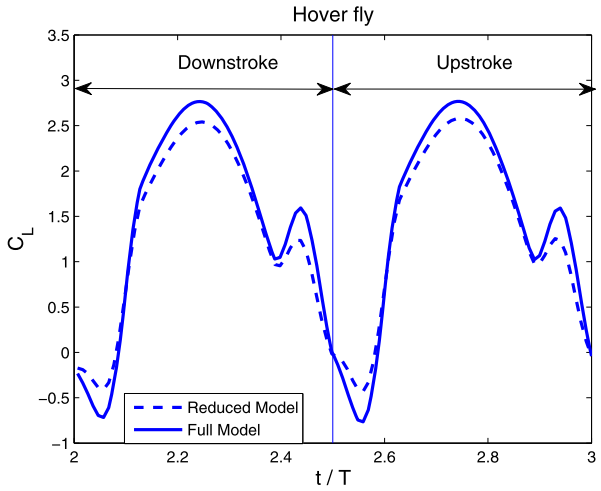

(c) Hover fly, $f = 160$ Hz and $\alpha_m = 29°$

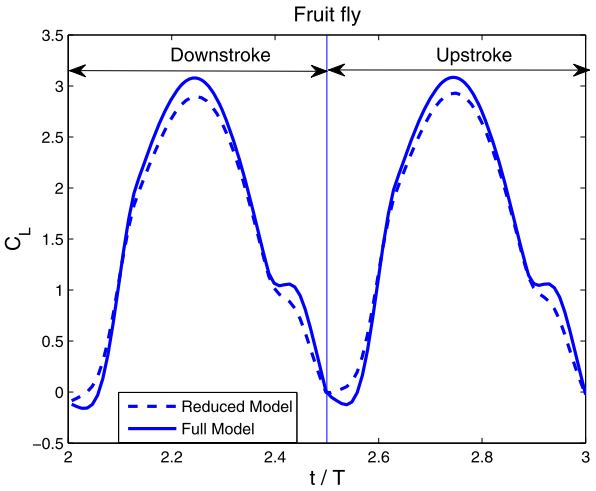

(d) Fruit fly, $f = 254$ Hz and $\alpha_m = 46°$

Fig. 7. Results for the C_L build up throughout the cycle using the reduced-order model versus the full model.

6. Conclusion

This work provides a state-space model for the unsteady lift due to flapping flight. The model is based on an extension to Duhamel's principle to non-conventional lift curves with the specific objective of capturing the contribution of the Leading Edge Vortex (LEV). The unsteady lift due to arbitrary wing motion is generated using the static lift curve. The effects of the aspect ratio on the empirical formulae used to predict the static lift due to a stabilized LEV were also accounted for.

The derived model is validated through a comparison with direct numerical simulations of Navier–Stokes on hovering insects. The results show that the lift variation throughout the flapping cycle matches well those of the benchmark results for all insects. A comparison with quasi-steady models that capture the LEV contribution is performed to assess the role of unsteadiness. The results show that quasi-steady models, which capture the LEV contribution, result in higher aerodynamic loads. Deviations up to 16.9% in cycle-average lift coefficients and 31.6% in root-mean-squared errors of the lift coefficient were found using those quasi-steady models. On the other hand, a comparison with classical unsteady approaches is also presented to assess the LEV dominance. We found that the classical unsteady approaches overestimate the aerodynamic loads, particularly at high angles of attack. They perform well near stroke reversals where the rotational contribution is dominant. Deviations of the classical unsteady approach from the direct numerical simulations were up to 49.2% in cycle-average lift coefficients and 36.2% in root-mean-squared errors of the lift coefficient.

The derived model can be considered as a blend of the classical unsteady aerodynamic models and the quasi-steady models that capture the LEV contribution. Therefore, it performs better than the two and requires almost the same computational cost. In terms of the comparison metrics, the deviation of the derived model from the DNS results ranges between 0.3%–7.3% in the cycle-average lift coefficients and between 5.8%–12.8% in root-mean-squared errors of the lift coefficient. Finally, a reduced-order model consisting of four internal aerodynamic states is derived from the full model (100 states) for flight dynamics and control analyses. The resulted lift coefficient using the reduced-order model is in a very good agreement with that of the full model.

Acknowledgements

The first author acknowledges Mostafa Ramadan at the University of Manchester for his valuable discussions about determination of the static lift coefficients and the morphological parameters of the insects. This work has been approved for public release; distribution unlimited per 88ABW-2013-4339.

References

[1] I.H. Abbott, A.E. Von Doenhoff, Theory of Wing Sections, Dover Publications, New York, 1959.
[2] A. Andersen, U. Pesavento, Z. Wang, Unsteady aerodynamics of fluttering and tumbling plates, J. Fluid Mech. 541 (2005) 65–90.
[3] A. Andersen, U. Pesavento, Z.J. Wang, Analysis of transitions between fluttering, tumbling and steady descent of falling cards, J. Fluid Mech. 541 (2005) 91–104.
[4] S.A. Ansari, R. Zbikowski, K. Knowles, Aerodynamic modelling of insect-like flapping flight for micro air vehicles, Prog. Aerosp. Sci. 42 (2006) 129–172.
[5] S.A. Ansari, R. Zbikowski, K. Knowles, Non-linear unsteady aerodynamic model for insect-like flapping wings in the hover. Part 1: Methodology and analysis, J. Aerosp. Eng. 220 (2006) 61–83.
[6] S.A. Ansari, R. Zbikowski, K. Knowles, Non-linear unsteady aerodynamic model for insect-like flapping wings in the hover. Part 2: Implementation and validation, J. Aerosp. Eng. 220 (2006) 169–186.
[7] T.S. Beddoes, Representation of airfoil behavior, Vertica 7 (2) (1983) 183–197.
[8] G.J. Berman, Z.J. Wang, Energy-minimizing kinematics in hovering insect flight, J. Fluid Mech. 582 (1) (2007) 153–168.
[9] R.L. Bisplinghoff, H. Ashley, R.L. Halfman, Aeroelasticity, Dover Publications, New York, 1996.
[10] S.L. Brunton, C.W. Rowley, Empirical state-space representations for Theodorsen's lift model, J. Fluids Struct. 38 (2013) 174–186.
[11] T. Cebeci, M. Platzer, H. Chen, K.-C. Chang, J.P. Shao, Analysis of Low Speed Unsteady Airfoil Flows, Horizons Publishing Inc./Springer, Long Beach/Berlin, Heidelberg, New York, 2005.
[12] R. Demoll, Der Flug Der Insekten und Der Vogel, G. Fischer, Jena, 1918.
[13] R. Demoll, Der Flug Der Insekten, Naturewissenschaften 7 (1919) 480–481.
[14] X. Deng, L. Schenato, W.C. Wu, S.S. Sastry, Flapping flight for biomimetic robotic insects. Part I: System modeling, IEEE Trans. Robot. 22 (4) (2006) 776–788.
[15] M.H. Dickinson, F.-O. Lehmann, S.P. Sane, Wing rotation and the aerodynamic basis of insect flight, Science 284 (5422) (1999) 1954–1960.
[16] D.B. Doman, M.W. Oppenheimer, D.O. Sigthorsson, Wingbeat shape modulation for flapping-wing micro-air-vehicle control during hover, J. Guid. Control Dyn. 33 (3) (2010) 724–739.
[17] R. Dudley, C.P. Ellington, Mechanics of forward flight in bumblebees II. Quasi-steady lift and power requirements, J. Exp. Biol. 148 (1990) 53–88.
[18] C.P. Ellington, The aerodynamics of hovering insect flight II. Morphological parameters, Philos. Trans. R. Soc. Lond., Ser. B 305 (1984) 17–40.
[19] C.P. Ellington, The aerodynamics of hovering insect flight III. Kinematics, Philos. Trans. R. Soc. Lond., Ser. B 305 (1984) 41–78.
[20] C.P. Ellington, C.V. den Berg, A.P. Willmott, A.L.R. Thomas, Leading-edge vortices in insect flight, Nature 384 (1996) 626–630.
[21] A.R. Ennos, The kinematics and aerodynamics of the free flight of some diptera, J. Exp. Biol. 142 (1989) 49–85.
[22] Y.C. Fung, An Introduction to the Theory of Aeroelasticity, Dover, New York, 1969.
[23] I.E. Garrick, On some reciprocal relations in the theory of nonstationary flows, Tech. Rep. 629, NACA, 1938.
[24] R.T. Jones, Operational treatment of the nonuniform lift theory to airplane dynamics, Tech. Rep. 667, NACA, 1938.
[25] R.T. Jones, The unsteady lift of a finite wing, Tech. Rep. 682, NACA, 1939.
[26] R.T. Jones, The unsteady lift of a wing of finite aspect ratio, Tech. Rep. 681, NACA, 1940.
[27] W.P. Jones, Aerodynamic forces on wings in non-uniform motion, Tech. Rep. 2117, British Aeronautical Research Council, 1945.
[28] J.G. Leishman, T.S. Beddoes, A generalized model for unsteady aerodynamic behavior and dynamic stall using the indicial method, in: 42nd Annual Forum of the American Helicopter Society, Washington D.C., June 1986.
[29] J.G. Leishman, G.L. Crouse, State-space model for unsteady airfoil behavior and dynamic stall, AIAA paper 89-1319, 1989, pp. 1372–1383.
[30] J.G. Leishman, K.Q. Nguyen, State-space representation of unsteady airfoil behavior, AIAA J. 28 (5) (1990) 836–844.
[31] T.H. Mueller, Fixed and Flapping Wing Aerodynamics for Micro Air Vehicles Applications, AIAA Inc., 2001.
[32] M.W. Oppenheimer, D.B. Doman, D.O. Sigthorsson, Dynamics and control of a biomimetic vehicle using biased wingbeat forcing functions, J. Guid. Control Dyn. 34 (1) (2011) 204–217.
[33] U. Pesavento, Z.J. Wang, Navier–Stokes solutions, model of fluid forces, and center of mass elevation, Phys. Rev. Lett. 93 (2004).
[34] D.A. Peters, Two-dimensional incompressible unsteady airfoil theory—an overview, J. Fluids Struct. 24 (2008) 295–312.
[35] D.A. Peters, D. Barwey, M.J. Johnson, Finite-state airloads modeling with compressibility and unsteady free-stream, in: Sixth International Workshop on Dynamics and Aeroelastic Stability Modelling of Rotorcraft systems, UCLA, 1995.
[36] D.A. Peters, M.J. Johnson, Finite-state airloads for deformable airfoils on fixed and rotating wings, in: Aeroelasticity and Fluid/Structures Interaction Problems, a Mini-Symposium, 44 Annual Meeting, Chicago, 1994, pp. 1–28.
[37] D.A. Peters, S. Karunamoorthy, State-space inflow models for rotor aeroelasticity, in: Proceedings of the Holt Ashley 70th Anniversary Symposium, Stanford University, 1993.
[38] D.A. Peters, S. Karunamoorthy, State-space inflow models for rotor aeroelasticity, AIAA paper 94-1920-CP, 1994.
[39] D.A. Peters, S. Karunamoorthy, W. Cao, Finite-state induced flow models, Part I: Two-dimensional thin airfoil, J. Aircr. 44 (1995) 1–28.
[40] E.C. Polhamus, A concept of the vortex lift of sharp-edge delta wings based on a leading-edge-suction analogy, Tech. Rep. NASA TN D-3767, Langely Research Center, Langely Station, Hampton, VA, 1966.
[41] E. Reissner, Effect of finite span on the air load distributions for oscillating wings, I – Aerodynamic theory of oscillating wings of finite span, Tech. Rep. 1194, NACA, 1947.
[42] S.P. Sane, The aerodynamics of insect flight, J. Exp. Biol. 206 (2003) 4191–4208.
[43] S.P. Sane, M.H. Dickinson, The aerodynamic effects of wing rotation and a revised quasi-steady model of flapping flight, J. Exp. Biol. 205 (2002) 1087–1096.
[44] L. Schenato, D. Campolo, S.S. Sastry, Controllability issues in flapping flight for biomimetic MAVs, in: 42nd IEEE Conference on Decision and Control, vol. 6, 2003, pp. 6441–6447.
[45] H. Schlichting, E. Truckenbrodt, Aerodynamics of the Airplane, McGraw-Hill, 1979.
[46] W. Shyy, Y. Lian, J. Tang, D. Viiero, H. Liu, Aerodynamics of Low Reynolds Number Flyers, Cambridge University Press, 2008.
[47] W. Su, C.E.S. Cesnik, Coupled nonlinear aeroelastic and flight dynamic simulation of a flapping wing micro airvehicle, in: International Forum on Aeroelasticity and Structural Dynamics, 2009.
[48] W. Su, C.E.S. Cesnik, Flight dynamic stability of a flapping wing MAV in hover, AIAA paper 2011-2009, Apr. 2011.
[49] M. Sun, G. Du, Lift and power requirements of hovering insect flight, Acta Mech. Sin. 19 (5) (2003) 458–469.
[50] H.E. Taha, M.R. Hajj, A.H. Nayfeh, Flight dynamics and control of flapping-wing MAVs: a review, Nonlinear Dyn. 70 (2) (2012) 907–939.
[51] T. Theodorsen, General theory of aerodynamic instability and the mechanism of flutter, Tech. Rep. 496, NACA, 1935.
[52] J.R. Usherwood, C.P. Ellington, The aerodynamics of revolving wings I. Model hawk moth wings, J. Exp. Biol. 205 (2002).
[53] C. Van den Berg, C.P. Ellington, The three-dimensional leading-edge vortex of a hovering model hawk moth, Philos. Trans. R. Soc. Lond., Ser. B 352 (1997) 329–340.
[54] C. Van den Berg, C.P. Ellington, The vortex wake of a hovering model hawk moth, Philos. Trans. R. Soc. Lond., Ser. B 352 (1997) 317–328.
[55] B. Van der Wall, J.G. Leishman, The influence of variable flow velocity on unsteady airfoil behavior, J. Am. Helicopter Soc. 39 (4) (1994).
[56] H. Wagner, Uber die Entstehung des dynamischen Auftriebs von Tragflugeln, Z. Angew. Math. Mech. 5 (1925).
[57] Z.J. Wang, Dissecting insect flight, Annu. Rev. Fluid Mech. 37 (2005) 183–210.
[58] Z.J. Wang, J.M. Birch, M.H. Dickinson, Unsteady forces in hovering flight: computation vs experiments, J. Exp. Biol. 207 (2004) 449–460.
[59] C. Wang, J.D. Eldredge, Low-order phenomenological modeling of leading-edge vortex formation, Theor. Comput. Fluid Dyn. (2012) 1–22.
[60] T. Weis-Fogh, Quick estimates of flight fitness in hovering animals, including novel mechanisms for lift production, J. Exp. Biol. 59 (1) (1973) 169–230.
[61] A.P. Willmott, C.P. Ellington, A.L.R. Thomas, Flow visualization and unsteady aerodynamics in the flight of the hawk moth Manduca sexta, Philos. Trans. R. Soc. Lond., Ser. B 352 (1997) 303–316.